

On Thermally Controlled Light Propagation in Plasmonics Waveguide and Filter

Mehdi Afshari-Bavil¹, Nader Daneshfar¹, Dong Liu^{2*}

¹Department of Physics, Faculty of Science, Razi University, Kermanshah, Iran

²Key Laboratory of Atmospheric Optics, Anhui Institute of Optics and Fine Mechanics, Chinese Academy of Sciences, Hefei, Anhui 230031, China

***Corresponding author:** Dong Liu, Key Laboratory of Atmospheric Optics, Anhui Institute of Optics and Fine Mechanics, Chinese Academy of Sciences, Hefei, Anhui 230031, China, E-mail: dliu@aiofm.cas.cn

Received date: 15-October-2022, Manuscript No. tspa-22-77299; **Editor assigned:** 18-October-2022, PreQC No. tspa-22-77299 (PQ); **Reviewed:** 25-October-2022, QC No. tspa-22-77299 (Q); **Revised:** 30-October-2022, Manuscript No. tspa-22-77299 (R); **Published:** 2-November-2022, DOI. 10.37532/2320-6756.2022.10(11).309

Abstract

An active ultra-compact plasmonic waveguide composed of a subwavelength slit and perforated in Vanadium Dioxide (VO_2) followed by a metallic layer is proposed and numerically analyzed. Refractive index variation of VO_2 by external stimuli provides a feasible way for tuning the optical properties of the waveguide. Varying the refractive index of VO_2 corresponds with changing the phase of VO_2 to the metallic state (“on” state). Consequently, the entire structure becomes a typical Metal-Insulator-Metal (MIM) waveguide that routes the incident light through the slit. In addition, during the “off” state, the incident light thereby propagates in the slit and VO_2 medium and mitigates rapidly. By adding a MIM waveguide attached to the Fabry-Perot (FP) cavity, spectrally wide stopband and passband filtering features in the telecommunication frequency regime are demonstrated. Tailoring the resonance wavelength can be performed through the geometrical parameters. Such active plasmonic waveguides with high transmission, coupling, and compact size can be utilized in future fully integrated all plasmonic chip technology.

Keywords: Plasmonics; Waveguide; Filter; Vanadium dioxide

Introduction

Plasmonics is a potential device technology to control light in sub-diffraction regime with sufficiently high physical features and minimized geometry [1, 2]. This natural light squeezing character of surface plasmon beyond the diffraction limit has attracted great interest in developing optical chip minimization with high responsivity and low energy consumption [3-8]. Various developed plasmonic devices such as waveguides, photodetectors, modulators, filters, and lensing have been numerically and/or experimentally demonstrated [5, 13-24]. For light propagation, different types of wave-guiding structures have been introduced. One of the popular wave-guiding configurations is Metal-Insulator-Metal (MIM) structure that is compatible with the complementary metal-oxide-semiconductor platform [1].

Citation: Dong Liu. On Thermally Controlled Light Propagation in Plasmonics Waveguide and Filter.2022;10(11):309.

©2022 Trade Science Inc.

However, modulating light propagation in different conditions by external stimuli to achieve a plasmonic chip is challenging. Tremendous progress has been accomplished in achieving active plasmonic devices, particularly waveguides and filters [25-27]. Tunable Surface Plasmon Polariton (SPP) devices by using liquid crystals, electro optical materials, shape memory alloys, photoacoustic materials, liquid metals, piezo-electric materials, and Phase Change Materials (PCM) have been widely demonstrated. PCM materials play a vital role because of their distinct status under various irritants, such as heat, strain, voltage, optical pumping, and current.

Volatile PCMs such as Vanadium Dioxide (VO_2) which switches between two recognizable insulators and a metallic phase on a picosecond scale, have a superior characteristic in the telecommunication regime compared with nonvolatile PCMs such as GeSbTe , which switches between crystalline and amorphous states [28-30]. VO_2 has sharp variation in its refractive index when undergoing transition from insulator to the metallic phase [31]. The transition occurs when VO_2 is agitated by a stimulus, which increases the temperature beyond the phase-transition temperature of 68°C [32]. Considering that the VO_2 layer is a film without further implementation, the agitation straightforwardly can be accomplished by direct heating to increase the temperature. The transition is reversible on a picosecond time scale. Quantifying this transition is introduced by the mechanism based on Peierls instability coupled with an enharmonic phonon contribution [32]. The refractive index for VO_2 at telecommunication and infrared regime is adapted from experimental results [33]. In telecommunication regime in the insulator phase, the refractive index is approximately $3+0.4i$, and it becomes $2+3i$ in the metallic phase [33]. Qualitatively, the effective dielectric function of VO_2 at intermediate temperature is introduced by using Bruggeman effective medium theories [34]. Recently, several thermally controlled plasmonic structures based on VO_2 have been proposed and experimentally demonstrated [31].

Passive plasmonic filters have been widely demonstrated theoretically and experimentally to achieve stop or pass wavelength selection [35-37]. Active filters are mandatory to seamlessly integrate plasmonic components into a compact chip. Considerable efforts are dedicated in achieving tunable plasmonic filters [19, 38-41]. Recently, a tunable and highly efficient but slightly compact graphene-based band-stop filter composed of a periodic structure based on bilayer graphene nanoribbons in the mid-infrared region is demonstrated [38]. The filter is tuned over a wide range under applied voltage varying from 1 V to 5 V.

In this paper, first, we studied a VO_2 -based waveguide (VIV) features under applied heat to achieve off and on states. The transmission is measured by a numerical approach based on the Finite Element Method (FEM). Then, we added a FP resonator along the MIM waveguide to design a wide stopband filter and determined on/off transmission features. Finally, the structure is modified to operate as active passband in on/off states. Given the simple configuration and compact size, a wave guiding and filtering structure can be easily fabricated and highly integrated with other plasmonic devices on a chip.

Structure Description and Theoretical Model

As shown in **FIG. 1**, our proposed plasmonic waveguide is composed of two successive VIV and MIM waveguides, and p-polarized light is concentrated into the slit from Si-wire taper waveguide. The widths of VIV and MIM waveguides are equal and represented by W , and the length of VIV and MIM waveguides is represented by h and L , respectively. The refractive index data of

VO₂ is adapted from the experimental work reported by Joushaghani *et al.* [33]. For telecommunication regime, the refractive index of insulator VO₂ is approximately 3+0.4i, whereas it is n=2+3i for the metallic VO₂ [33]. The permittivity of silver is characterized by the Drude model:

$$\epsilon = \epsilon_{\infty} - \frac{\omega_p^2}{\omega^2 + i\omega\Gamma} \quad (1)$$

where ϵ_{∞} , ω_p , and Γ stand for high-frequency bulk permittivity, bulk plasmon frequency, and electron collision frequency, respectively, which are set as 4.2, 1.346×10^{16} rad/s, and 9.617×10^{13} rad/s [42]. The insulator layer operates as a core; thus, narrower cores have stronger confinement. When VO₂ is in the metallic phase, for cores smaller than the incident wavelength, only one propagation mode is identified, where its propagation constant (β) can be determined by solving the dispersion relation [43, 44]:

$$k_{vm} + \epsilon_{vm} k_d \tanh\left(\frac{k_d w}{2}\right) = 0 \quad (2)$$

Where k_{vm} and k_d are defined as $k_d = (\beta^2 - k_0^2)^{1/2}$ and $k_{vm} = (\beta^2 - \epsilon_{vm} k_0^2)^{1/2}$, and $k_0 = 2\pi / \lambda$ is the free space wave vector, and ϵ_v is the permittivity of VO₂ in the metallic phase. Light experiences larger refractive index inside the waveguide because of light squeezing and other observed phenomena, which is known as the effective refractive index. The fabrication process of proposed design is straightforward; first, the silver layer is deposited on the substrate by sputtering technique, and then the VO₂ film is attached by using lithography or deposition techniques. Finally, the slit is perforated by using ion beam milling. The present study is carried out by using Finite Element Method (FEM) for the proposed device in the Radio Frequency (RF) module of COMSOL Multiphysics software.

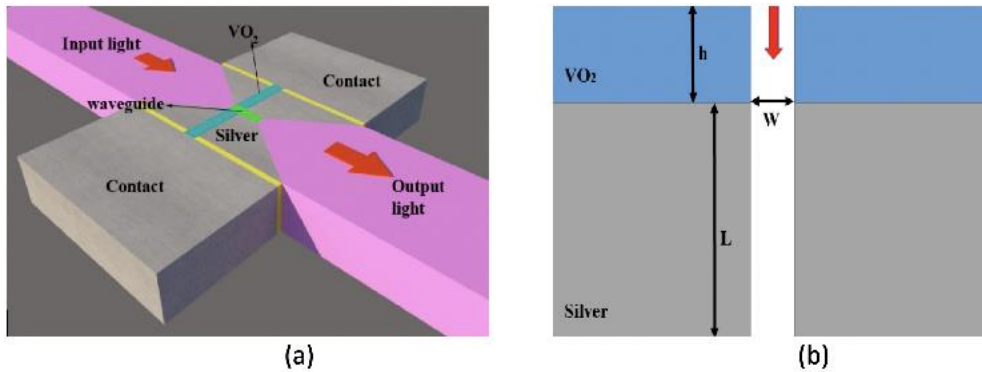


FIG.1(a) Schematic of the proposed structure. (b) W, h, L stands for waveguide width, VIV waveguide length and MIM waveguide length, respectively. The P-polarized incident light is coupled to the waveguide from Si nanowire taper.

Simulation Results and Analysis

In the simulation, the fundamental TM mode of the waveguide is excited by a pulse dipole source from the taper on the left and coupled to the waveguide in the VO₂ medium. P and Q are set as the entrance and exit ports of waveguide to detect the transmitted powers of P_{in} and P_{tr} and calculate the transmission of two power monitors. Transmission is defined as $T=P_{tr}/P_{in}$. The absorption

parameter, which is a measurement of dissipation of the power in the device, can be simply deduced by $A=I-R-T$, where R is the reflection. The geometrical parameters of the structure are set to be $W=150$ nm, $h=600$ nm, and $L=1100$ nm. When the structure is in off state (no heating is applied), light transmission through the waveguide is negligible. For insulator VO_2 , the VIV waveguide becomes a dielectric waveguide because near refractive indexes of the media light cannot confine and propagate through it. When heat is applied to the structure, VO_2 undergoes a transition and becomes metal, and light properly propagates through it. **FIG. 2(a)** depicts the transmission in the insulator and metal phases. It is seen that for wide wavelength range, the transmission in the metal state is considerably high, whereas in the insulator state, the transmission dropped notably. **FIG. 2b and 2c** represents the magnetic field distribution in both metallic (ON) and insulator (OFF) states. In the metallic state, light propagates normally, whereas in the insulator state, light is not confined inside the waveguide, and it propagates in the entire VO_2 medium.

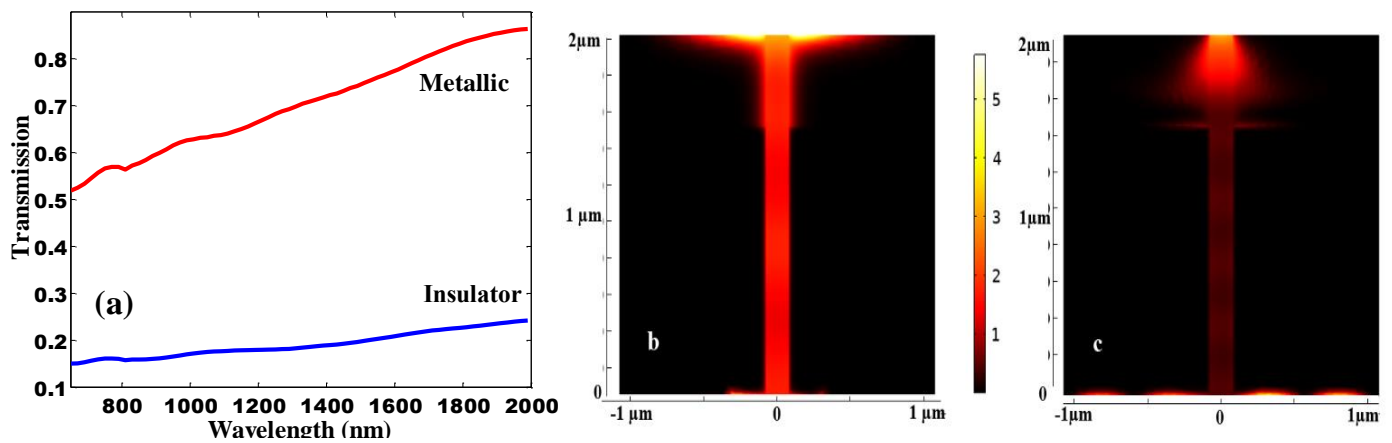


FIG. 2(a) Transmission profile when VO_2 is in metallic (ON) and insulator (OFF) phase. (b) Magnetic field distribution when VO_2 is in metallic phase. (c) Magnetic field distribution when VO_2 is in insulator phase.

The length of the VIV and MIM layers can affect the transmission features. The longer the VIV, the more dissipation occurs and the lower the transmission. **FIGS. 3a and 3b** show the transmission profile *versus* different VIV and MIM lengths. Longer VIV decreases the transmission in the metallic and insulator phases. Based on our requirement, suitable compromising should be conducted. By contrast, the transmission is not affected notably by the MIM length. However, MIM waveguides larger than the SPP propagation length because of inherent loss of metal will decrease the transmission. **FIG. 3(c)** shows the transmission profile *versus* the waveguide width. The narrower the waveguides, the less power is transmitted; hence, less transmission occurs.

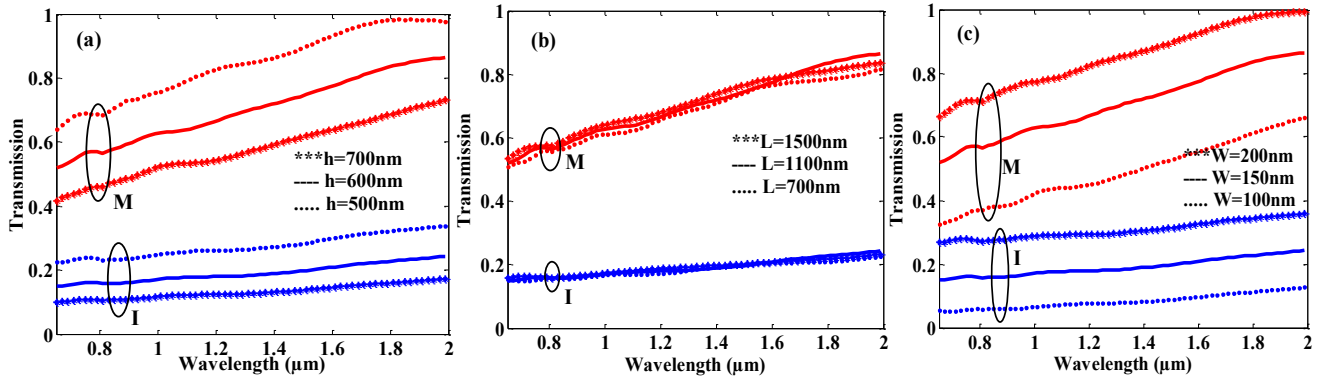


FIG. 3 Spectral dependence of transmission for various (a) VO₂ waveguide length, (b) Metallic waveguide Length, and (c) waveguide width. It can be seen that MIM length doesn't affect the transmission.

In optical chips light transmission at a specific wavelength be blocked. Different configuration has been proposed as passive stopband structures. Most popular structures are designed by employing FP cavities. If the FP cavity locates in the vicinity of a waveguide, then it can confine portion of the propagating light within the waveguide. This light confinement merely occurs at some specific wavelengths corresponding to resonance wavelength of the cavity. The resonant condition that can determine the resonant wavelength can be determined through the following equation [45]:

$$2 \frac{2\pi}{\lambda_m} \text{Re}(N_{\text{eff}})d + \Delta\phi = 2m\pi \tag{3}$$

where d is the FP cavity length; N_{eff} is the effective refractive index of the cavity, and $\Delta\phi$ is the phase shift of the beam, which experiences reflection on the two end facets of the cavity. The positive integer m represents the number of antinodes of the standing wave. λ_m straightforwardly can be calculated using equation 3. We embedded the FP cavity in our waveguide structure to obtain an active stop band filter (FIG. 4a). d and t stand for cavity length and width, respectively, which are set as 580 nm and 150 nm, respectively, whereas the gap is fixed at 10 nm. FIG. 4b depicts the transmission profile; when heat is applied, the VO₂ becomes metal. Two resonances corresponding to the resonance wavelength of the cavity are distinct on the plot. For these resonances, the transmission drops sharply. The blue line shows the transmission when heating is OFF and VO₂ is in the insulator phase. Magnetic field distributions for resonance wavelength in the metallic and insulator phases of VO₂ are presented in FIGS. 4c and 4d. Large portion of light trapped within the cavity and standing waves is created.

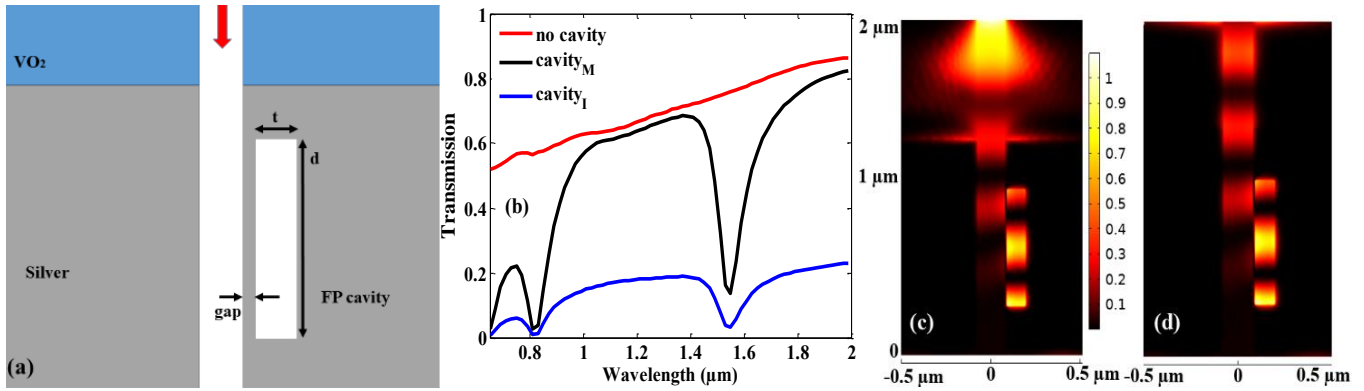


FIG 4. (a) 2D schematic of the proposed stop band filter. t and d stand for cavity length and width. The gap is considered to be 10 nm to ensure noticeable coupling. (b) transmission profile when VO₂ is in metallic and insulator phase. (c) Magnetic field distribution when VO₂ is in insulator mode (d) Magnetic field distribution when VO₂ is in metallic mode.

It is worthy to note that the resonance wavelengths directly depend on the cavity length (d), and the effective refractive index indirectly depends on the cavity width (t). Therefore, wavelength tuning can be performed through tailoring geometrical parameters of the cavity. The gap between the cavity and the waveguide is a critical parameter that can affect transmission intensity. FIG. 5a shows the transmission profile versus the cavity length, whereas FIG. 5b shows the transmission versus the cavity width. It can clearly be seen that there is a red-shift of the transmission spectrum as the length and width of cavity increases. Further, by increasing the length and width of cavity, the transmission intensity increases. For any desired resonance wavelength, the appropriate geometrical parameters can be adjusted. The penetration depth of SPP into silver is estimated to be less than 30 nm; therefore, considerable coupling the gap should be less than the penetration depth. FIG. 5c shows the gap thickness dependence of transmission. For narrower gaps, the cavity can trap the light considerably. The wider the gap, the less the light confinement.

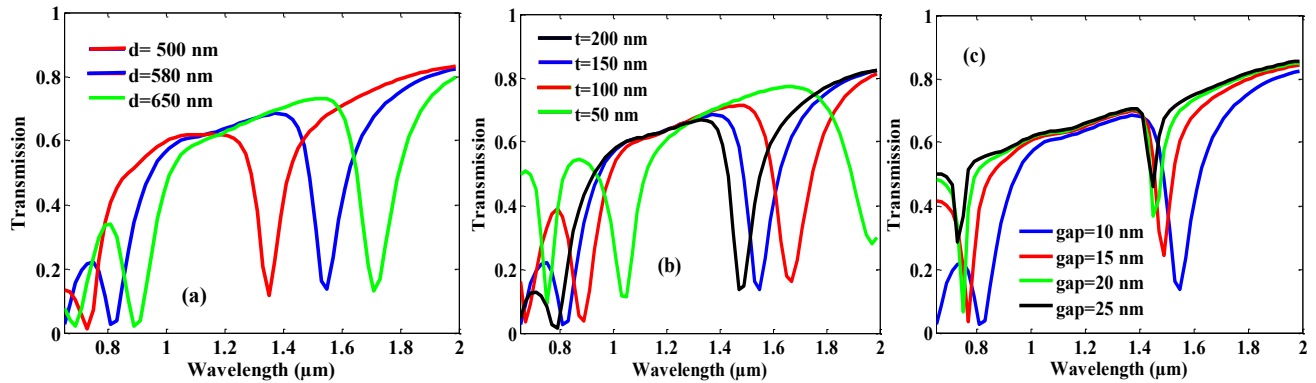


FIG. 5(a) Spectral dependence of transmission for various (a) FP cavity length, (b) FP cavity width, and (c) the gap between cavity and waveguide.

In the next step, we modified our structure to design a passband filter. We utilized the FP cavity in the waveguide to permit light propagation in specific wavelengths. The structure is shown in FIG. 6a. The FP cavity is embedded inside the waveguide with two narrow separating gaps. The resonance condition and propagation mechanism are similar to the stopband filter, which can be estimated using equation 3. In the transmission profile depicted in FIG. 6b, two peaks correspond to the resonance wavelength of

the cavity can be seen. The black line shows the transmission when VO₂ is in the metallic phase, whereas the blue line indicates transmission in the insulator phase. The red line shows the transmission when no cavity is presented. In general, the presence of cavities leads to light propagation and decreases the transmission. **FIG. 6c** shows the magnetic field distribution in resonance wavelength and the standing waves inside the cavity.

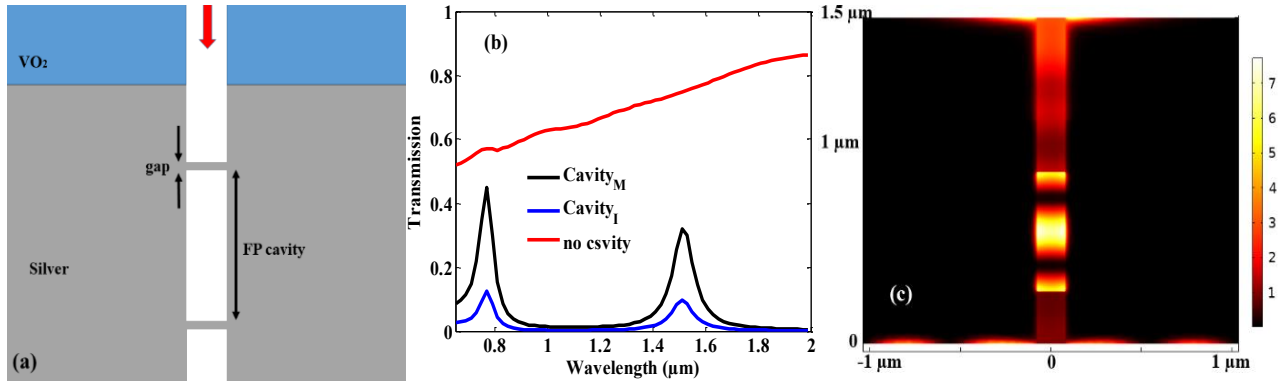


FIG. 6 (a) 2D schematic of the proposed passband filter. The gap is considered to be 10 nm to ensure noticeable coupling. (b) transmission profile when VO₂ is in metallic and insulator phase. (c) Magnetic field distribution when VO₂ is in metallic mode.

The above mentioned structure based on geometrical parameters has various resonances. Another configuration also shows stop band behavior (**FIG. 7a**). This structure has features that depend on input-output location, which can permit only one resonance coupling to the output port (**FIG. 7b**) and field distribution (**FIG. 7c**). Fei investigated the transmission behavior by the arbitrary input position and superposition of magnetic fields inside the cavity and determined in what input positions single resonance can be seen [45,46]. When input is at the center of the cavity, only first resonance will be presented (B point). For locations, where the input port is on both end sides of the cavity, both resonances will occur (A and C). However, if the input moves from the center about $d/4$, then the second resonance will be propagated. Moreover, by placing two outputs in different locations, the propagation at specific wavelength through the particular output can occur.

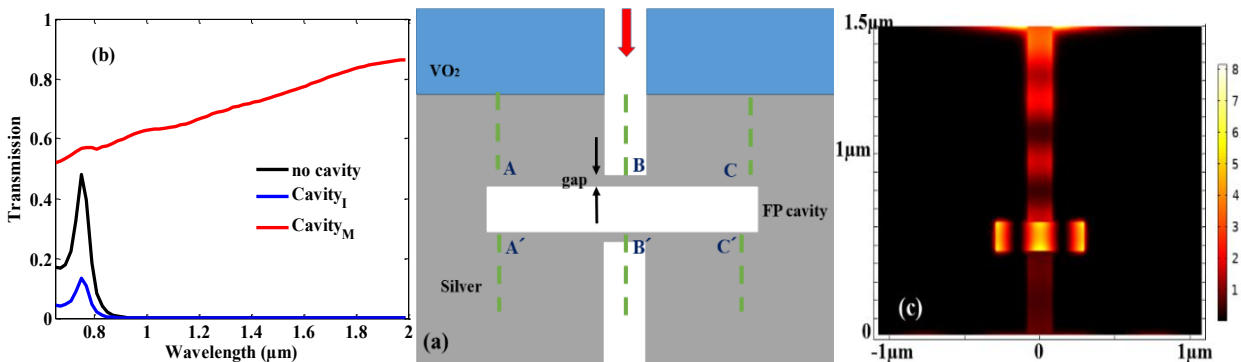


FIG. 7(a) 2D schematic of the proposed passband filter. The gap is considered to be 10 nm to ensure noticeable coupling. (b) transmission profile when VO₂ is in metallic and insulator phase. (c) Magnetic field distribution when VO₂ is in metallic mode.

The two above mentioned configurations despite their lower transmission present a narrow transmission profile. The output port is

modified to increase the transmission to two locations of the cavity (**FIG. 8a**). Ports and cavity are in parallel and located in a way that the bottom of the input port axes is under the cavity's center. In addition, top of output port is above the center of the cavity. This difference in location is represented by ΔL in the picture and set as 250 nm. The width of the input, cavity, and output ports are represented by W_1 , W_2 , and W_3 , respectively. In general, W_1 and W_3 are equal to the modified width of the cavity. The transmission profile is depicted in **FIG. 8b**. The transmission (black line) output widths, when W_2 is equal to the input, are increased slightly; however, the profile is broadened and red-shifted. Green and C lines show the transmission when W_2 is set as 100 nm and 50 nm. According to the resonance condition of the cavity, any changes in the cavity width will result in different effective refractive indices and correspondingly different resonance wavelengths. Furthermore, the narrow cavities have less coupling. **FIG. 8c** shows the magnetic field distribution at resonance wavelength. Standing waves inside the cavity can be seen. According to our experimental obstacles, proper arrangement can be considered, and desired resonance wavelength can be tuned.

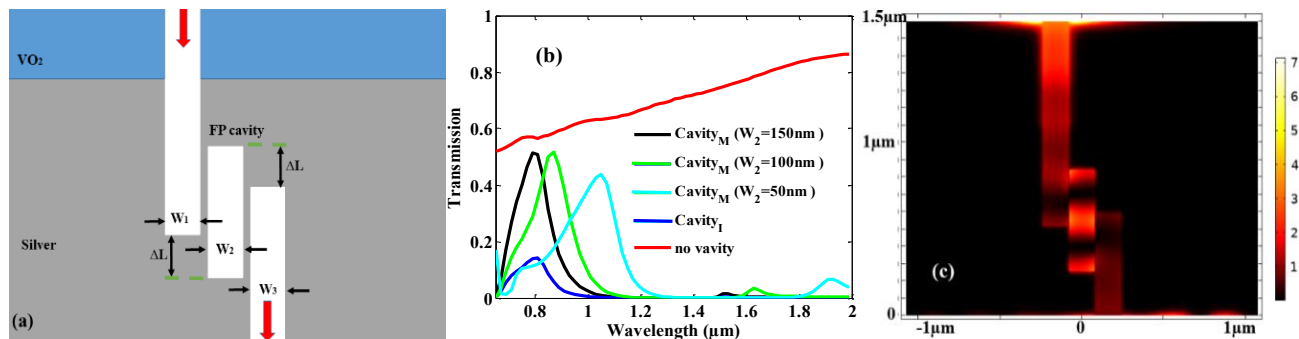


FIG.8(a) 2D schematic of the proposed passband filter. The gap is considered to be 10 nm to ensure noticeable coupling. (b) transmission profile when VO₂ is in metallic and insulator phase. (c) Magnetic field distribution when VO₂ is in metallic mode.

Conclusion

In conclusion, an active subwavelength plasmonic waveguide, stopband, and passband filter are proposed by using PCM and Fabry Perot cavity and theoretically and numerically investigated. ON and OFF states that are created by introducing heat to the system showed two distinct features when VO₂ was in the metallic or insulator state. The role of the geometrical parameters is determined in wave guiding features. Furthermore, the filtering characteristics of both filters are studied, and different arrangements based on the location of input, output, and cavity are also presented. Given this simple configuration, the structure has high potential and feasibility to be integrated into nanoscale plasmonic chips and circuits.

Declarations

Funding

The authors did not receive support from any organization for the submitted work.

Conflicts of interest

The authors have no conflicts of interest to declare that are relevant to the content of this article.

Availability of data and material

The data presented in this study are available on request from the corresponding author.

Code availability

The code used in this study are available on request from the corresponding author.

Authors' contributions

The corresponding author is responsible for ensuring that the descriptions are accurate and agreed by all authors.

Ethics approval

Not applicable.

Consent to participate

Not applicable.

Consent for publication

Not applicable.

REFERENCES

1. Maier SA. Plasmonics: fundamentals and applications. New York: springer; 2007.
2. Zayats AV, Maier S, editors. Active plasmonics and tuneable plasmonic metamaterials. John Wiley & Sons; 2013.
3. Afshari-Bavil M, Dong M, Li C, et al. Thermally controllable high-efficiency unidirectional coupling in a double-slit structure filled with phase change material. *IEEE Photonics J.* 2019;11(2):1-8.
4. Bavil MA, Deng Q, Zhou Z. Extraordinary transmission through gain-assisted silicon-based nanohole arrays in telecommunication regimes. *Opt Lett.* 2014;39(15):4506-9.
5. Wang X, Cheng Z, Xu K, et al. High-responsivity graphene/silicon-heterostructure waveguide photodetectors. *Nature Photonics.* 2013;7(11):888-91.
6. Bermúdez-Ureña E, Tutuncuoglu G, Cuerda J, et al. Plasmonic waveguide-integrated nanowire laser. *Nano lett.* 2017;17(2):747-54.
7. Joushaghani A, Jeong J, Paradis S, et al. Wavelength-size hybrid Si-VO₂ waveguide electroabsorption optical switches and photodetectors. *Opt Express.* 2015;23(3):3657-68.
8. Miller KJ, Hallman KA, Haglund RF, et al. Silicon waveguide optical switch with embedded phase change material. *Optics express.* 2017;25(22):26527-36.
9. HAL. Iang, RIS. Oref, JMU. Ianwei, et al. Using Three- and Four-Waveguide Directional Couplers. *Appl Opt.* 2015;54(19).
10. Cai W, Shin W, Fan S, et al. Elements for plasmonic nanocircuits with three-dimensional slot waveguides. *Adv Mater.* 2010;22(45):5120-4.
11. Ono M, Taniyama H, Kuramochi E, et al. Toward application of plasmonic waveguides to optical devices. *NTT Tech. Rev.* 2018;16(7):14-9.
12. Mirahmadi M, Mahinroosta T, Hamidi SM. Manipulating plasmon-exciton interactions in the plasmonic waveguide structure based on the dispersion relations concept. *Opt, Quantum Electron.* 2020;52(6):1-9.
13. Yang F, Cong H, Yu K, et al. Ultrathin broadband germanium-graphene hybrid photodetector with high performance. *ACS*

Appl Mater Interfaces. 2017;9(15):13422-9.

14. Dai X, Tchernycheva M, Soci C. Compound semiconductor nanowire photodetectors. In *Semiconductors Semimet.* 2016 (Vol. 94, pp. 75-107). Elsevier.
15. Sun M, Shieh W, Unnithan RR. Design of plasmonic modulators with vanadium dioxide on silicon-on-insulator. *IEEE Photonics J.* 2017;9(3):1-0.
16. Zhou G, Dai P, Wu J, et al. Broadband and high modulation-depth THz modulator using low bias controlled VO₂-integrated metasurface. *Opt Express.* 2017;25(15):17322-8.
17. Thomas R, Ikonic Z, Kelsall RW. Electro-optic metal-insulator-semiconductor-insulator-metal Mach-Zehnder plasmonic modulator. *Photonics Nanostructures-Fundam. Appl.* 2012;10(1):183-9.
18. J. K. Clark, Y. L. Ho, H. Matsui, et al. "Optically Pumped Hybrid Plasmonic-Photonic Waveguide Modulator Using the VO₂Metal-Insulator Phase Transition," *IEEE Photonics J.* 2018;10(1).
19. Trimby L, Baldycheva A, Wright CD. Phase-change band-pass filters for multispectral imaging. In *Photonic Phononic Prop. Eng. Nanostructures VIII 2018*(Vol. 10541, 148-155). SPIE.
20. Bavi MA, Sun X, Huang F. Classifying the transmission resonances of a subwavelength aperture within a thin metallic film by breaking the symmetry. *Phys. B: Condens Matter.* 2012;407(14):2768-72.
21. Foroughifar A, Saghaei H, Veisi E. Design and analysis of a novel four-channel optical filter using ring resonators and line defects in photonic crystal microstructure. *Opt Quantum Electron.* 2021;53(2):1-2.
22. Asl AB, Rostami A, Amiri IS. Terahertz band pass filter design using multilayer metamaterials. *Opt Quantum Electron.* 2020;52(3):1-3.
23. Ashari-Bavi M, Dong M, Li C, Feng S, et al. Compact plasmonic lens based on gradually decreasing size and separation nanohole cluster. *J Optics.* 2019;21(8): 085001.
24. Yuan GH, Rogers ET, Zheludev NI. Achromatic super-oscillatory lenses with sub-wavelength focusing. *Light: Sci Appl.* 2017;6(9):e17036.
25. Lu C, Hu X, Yang H, et al. Chip-integrated ultrawide-band all-optical logic comparator in plasmonic circuits. *Sci Rep.* 2014;4(1):1-8.
26. Emboras A, Hoessbacher C, Haffner C, et al. Electrically controlled plasmonic switches and modulators. *IEEE J. Sel. Top. Quantum Electron.* 2014;21(4):276-83.
27. Ding Y, Guan X, Zhu X, et al. Efficient electro-optic modulation in low-loss graphene-plasmonic slot waveguides. *Nanoscale.* 2017;9(40):15576-81.
28. Karimov KS, Mahroof-Tahir M, Saleem M, et al. Optical transmission in thin films of vanadium compounds. *J Semicond.* 2014;35(7):072002.
29. Karimov KS, Mahroof-Tahir M, Saleem M, et al. Temperature sensor based on composite film of vanadium complex (VO₂ (3-fl)) and CNT. *J. Semicond.* 2015;36(7):073004.
30. Li J, Liu B, Song Z, Yao D, et al. Reactive ion etching of Si₂Sb₂Te₅ in CF₄/Ar plasma for a nonvolatile phase-change memory device. *J Semicond.* 2013;34(5):056001.
31. Kocer H, Butun S, Banar B, et al. Thermal tuning of infrared resonant absorbers based on hybrid gold-VO₂ nanostructures. *Appl Phys Lett.* 2015;106(16):161104.
32. Budai JD, Hong J, Manley ME, et al. Metallization of vanadium dioxide driven by large phonon entropy. *Nature.* 2014;515(7528):535-9.

33. Joushaghani A. Arash Joushaghani A thesis submitted in conformity with the requirements for the degree of Doctorate of Philosophy Graduate Department of Electrical and Computer Engineering c Copyright 2014 by Arash Joushaghani Abstract (Doctoral dissertation, Thesis).
34. Jepsen PU, Fischer BM, Thoman A, et al. Metal-insulator phase transition in a VO₂ thin film observed with terahertz spectroscopy. *Phys Rev B*. 2006;74(20):205103.
35. Bavi MA, Gao L, Sun X. A compact nanoplasmonics filter and intersection structure based on utilizing a slot cavity and a Fabry-Perot resonator. *Plasmonics*. 2013;8(2):631-6.
36. Yun B, Hu G, Cui Y. A nanometric plasmonic waveguide filter based on Fabry-Perot resonator. *Opt Commun*. 2011;284(1):485-9.
37. McManamon PF, Dorschner TA, Corkum DL, et al. Optical phased array technology. *Proceedings of the IEEE*. 1996;84(2):268-98.
38. Wang X, Meng H, Liu S, et al. Tunable graphene-based mid-infrared plasmonic multispectral and narrow band-stop filter. *Mater Res Express*. 2018;5(4):045804.
39. Li W, Chang SJ, Wang XH, et al. A thermally tunable terahertz bandpass filter with insulator-metal phase transition of VO₂ thin film. *Opt Lett*. 2014;10(3):180-3.
40. Zhu Y, Vegesna S, Zhao Y, et al. Tunable dual-band terahertz metamaterial bandpass filters. *Opt Lett*. 2013;38(14):2382-4.
41. Ooi KJ, Bai P, Chu HS, et al. Ultracompact vanadium dioxide dual-mode plasmonic waveguide electroabsorption modulator. *Nanophotonics*. 2013;2(1):13-9.
42. Shuford KL, Ratner MA, Gray SK, et al. Finite-difference time-domain studies of light transmission through nanohole structures. *Appl Phys B*. 2006;84(1):11-8.
43. Dionne JA, Sweatlock LA, Atwater HA, et al. Plasmon slot waveguides: Towards chip-scale propagation with subwavelength-scale localization. *Phys Rev B*. 2006;73(3):035407.
44. Wang B, Wang GP. Plasmon Bragg reflectors and nanocavities on flat metallic surfaces. *Appl Phys Lett*. 2005;87(1):013107.
45. Hu F, Yi H, Zhou Z. Band-pass plasmonic slot filter with band selection and spectrally splitting capabilities. *Opt Express*. 2011;19(6):4848-55.
46. Nikitin SY, Lugovtsov AE, Priezzhev AV, et al. Relation between the diffraction pattern visibility and dispersion of particle sizes in an ektacytometer. *Quantum Electron*. 2011;41(9):843.